

HOW TO BUILD TATOOINE: REDUCING SECULAR EXCITATION IN *KEPLER* CIRCUMBINARY PLANET FORMATION

ROMAN R. RAFIKOV¹
Draft version May 4, 2021

ABSTRACT

Circumbinary planetary systems recently discovered by *Kepler* represent an important testbed for planet formation theories. Planetesimal growth in disks around binaries has been expected to be inhibited interior to ~ 10 AU by secular excitation of high relative velocities between planetesimals, leading to their collisional destruction (rather than agglomeration). Here we show that gravity of the gaseous circumbinary disk in which planets form drives fast precession of both the planetesimal and binary orbits, resulting in strong suppression of planetesimal eccentricities beyond 2-3 AU and making possible growth of $1 - 10^2$ km objects in this region. The precise location of the boundary of accretion-friendly region depends on the size of the inner disk cavity cleared by the binary torques and on the disk mass (even $0.01 M_{\odot}$ disk strongly suppresses planetesimal excitation), among other things. Precession of the orbit of the central binary, enhanced by the mass concentration naturally present at the inner edge of a circumbinary disk, plays key role in this suppression, which is a feature specific to the circumbinary planet formation.

Subject headings: planets and satellites: formation — protoplanetary disks — planetary systems — binaries: close

1. INTRODUCTION.

One of the most intriguing findings of the *Kepler* mission is the discovery of circumbinary planets around a sample of close binaries, affectionately termed *Tatooines* (Doyle et al. 2011; Welsh et al. 2012; Orosz et al. 2012a,b; Schwamb et al. 2012). Six such systems are known at the moment, with one of them, Kepler-47, harboring two planets (see Table 1). At least some of the *Kepler* circumbinary planets are likely in the Saturn or Jupiter mass regime. Semi-major axes of their orbits are typically small, $a_{pl} \lesssim 1$ AU, and close to the limit of dynamical stability (Holman & Wiegert 1999).

These systems provide interesting targets for testing our understanding of planet formation. It is generally agreed that in-situ formation of such planets is impossible because of the strong dynamical excitation due to central binary at their present locations (Meschiari 2012a; Paardekooper et al. 2012). The question typically addressed is at what separation could these planets form, subsequent to which they have migrated in. The bottleneck for planet formation here is the growth of $1 - 10^2$ km planetesimals, which is impossible if planetesimals have high eccentricities — instead of merging they get destroyed in high-speed collisions. Since the excitation by the binary is a rather long-range effect (in conventional secular theory eccentricity decays with distance only as r^{-1} , see equation (23)), it might easily be the case that the conditions for planetesimal growth are realized only beyond 10 AU (Moriwaki & Nakagawa 2004, hereafter MN04; Scholl et al. 2007). However, at such separations the timescale for growing massive cores capable of forming giant planets by core accretion may become prohibitive, especially if the lifetimes of *circumbinary* disks are shorter than around single stars. The latter seems to

be the case at least for the *circumstellar* disks in binaries (Cieza et al. 2009; Kraus et al. 2012).

Different ideas were proposed to alleviate this planetesimal fragmentation issue. Orbital alignment due to gas drag in presence of secular forcing has been suggested to facilitate growth of $1 - 10$ km bodies (Scholl et al. 2007), but this effect is size-dependent and does not work well for a broad spectrum of planetesimal masses. Paardekooper et al. (2012) explored very efficient accretion of dust by growing planetesimals as another way of bypassing the fragmentation problem.

In this work we show that gravitational effect of the circumbinary disk, in which planetesimals are immersed, modifies their secular excitation and significantly lowers their eccentricities beyond 2-4 AU from the star. Similar mechanism was invoked in Rafikov (2012b) to explain the origin of circumstellar planets on wide orbits (~ 2 AU) in small separation binaries, $a_b \approx 20$ AU. A unique feature of the circumbinary planet formation is that the effect of the disk gravity on the central binary often turns out being more important than the direct effect of the disk on planetesimal orbits. We now describe this idea in more detail.

2. SECULAR EVOLUTION.

We consider motion of massless planetesimals around a central binary. Binary has components with masses M_p and $M_s < M_p$ (mass ratio $\mu \equiv M_s/M_b < 1$, where $M_b = M_p + M_s$ is the binary mass), its semimajor axis and eccentricity are a_b and e_b correspondingly. For simplicity we will assume the disk to be axisymmetric with respect to the binary barycenter, i.e. the disk surface density is $\Sigma(r)$, where \mathbf{r} is the distance from the barycenter. Since we are primarily interested in the effect of the binary on planetesimal dynamics we neglect gas drag in this work (see §6). Planetesimals start on circular orbits and we are interested in their eccentricity evolution driven by the time-dependent and non-axisymmetric potential of

¹ Department of Astrophysical Sciences, Princeton University, Ivy Lane, Princeton, NJ 08540; rrr@astro.princeton.edu

Table 1
Circumbinary planetary systems

System	a_b (AU)	e_b	M_p (M_\odot)	M_s (M_\odot)	a_{pl} (AU)	a_{form}^a (AU)
Kepler-16 ¹	0.22	0.16	0.69	0.2	0.7	2.3-4.4
Kepler-34 ²	0.23	0.52	1.05	1.02	1.1	2.1-4.3
Kepler-35 ²	0.18	0.14	0.89	0.81	0.6	1.7-3.5
Kepler-38 ³	0.15	0.1	0.95	0.25	0.46	1.9-3.5
Kepler-47 ⁴	0.084	0.02	1.04	0.36	0.29 ^b	1.0-1.9
KIC 4862625 ⁵	0.17	0.21	1.38	0.39	0.63	2.7-5.1

¹Doyle et al. (2011); ²Welsh et al. (2012); ³Orosz et al. (2012b);

⁴Orosz et al. (2012a); ⁵Schwamb et al. (2012)

^a Inner edge of accretion-friendly zone, see §6

^b Semi-major axis of the inner planet

the binary.

Following MN04 we write down the equation of planetesimal motion as

$$\frac{d^2 \mathbf{r}}{dt^2} = -\frac{G(M_p + M_s)}{r^3} \mathbf{r} + \nabla R, \quad (1)$$

where the disturbing function R is

$$R = \frac{GM_p}{|\mathbf{r} - \mathbf{r}_p|} + \frac{GM_s}{|\mathbf{r} - \mathbf{r}_s|} - \frac{G(M_p + M_s)}{r} - U_d. \quad (2)$$

Here U_d is the disk potential and \mathbf{r}_p and \mathbf{r}_s are the vectors to primary and secondary from the barycenter of the binary.

Using Murray & Dermott (1999) we expand the disturbing function to second order in planetesimal and binary eccentricities e and e_b , retaining terms up to $O(e^2)$ and $O(ee_b)$, and then average it over the binary and planetesimal mean longitudes, thus eliminating short-period perturbations. We additionally expanded Laplace coefficients assuming $a_b/a \ll 1$, where a is the planetesimal semi-major axis. The resulting secular disturbing function R^{sec} is

$$R^{sec} = \frac{1}{2} a^2 n \dot{\omega}_d e^2 + \frac{\mu(1-\mu)}{4} n_b^2 a^2 \left(\frac{a_b}{a}\right)^5 \times \left[\frac{3}{2} e^2 + \frac{15}{4} (1-2\mu) \frac{a_b}{a} e e_b \cos(\varpi - \varpi_b) \right], \quad (3)$$

where we dropped insignificant e -independent terms. Here $n_b = (GM_b/a_b^3)^{1/2}$ is the binary mean motion,

$$\dot{\omega}_d = -\frac{1}{2nr^2} \frac{\partial}{\partial r} \left(r^2 \frac{\partial U_d}{\partial r} \right) \Big|_{r=a} \quad (4)$$

is the precession frequency of planetesimal orbit due to the disk potential, and $n = (GM_b/a^3)^{1/2}$ is the mean motion around a point mass $M_p + M_s$. To lowest order in e these expressions coincide with secular expansion of MN04, if we set $\dot{\omega}_d = 0$.

2.1. Evolution equations.

We now follow standard procedure (Murray & Dermott 1999) and introduce eccentricity vector $\mathbf{e} = (k, h) =$

$(e \cos \varpi, e \sin \varpi)$. Defining

$$A = \frac{3}{4} \mu (1-\mu) \frac{n_b^2}{n} \left(\frac{a_b}{a}\right)^5, \quad (5)$$

$$B = \frac{15}{16} \mu (1-\mu) (1-2\mu) \frac{n_b^2}{n} \left(\frac{a_b}{a}\right)^6 e_b, \quad (6)$$

we can write

$$\frac{R}{na^2} = \frac{A + \dot{\omega}_d}{2} (h^2 + k^2) + B(k \cos \varpi_b + h \sin \varpi_b). \quad (7)$$

This expression is accurate to $O(e_b^2)$. Evolution equations for h and k (Murray & Dermott 1999) attain a relatively simple form

$$\frac{dh}{dt} = (A + \dot{\omega}_d)k + B \cos \varpi_b, \quad (8)$$

$$\frac{dk}{dt} = -(A + \dot{\omega}_d)h - B \sin \varpi_b. \quad (9)$$

In the disk-free case ($\dot{\omega}_d = 0$) one recovers the secular evolution equations from MN04.

Now we introduce an important modification to the setup used in MN04. We assume that ϖ_b is not constant but *linearly increases with time* at constant rate $\dot{\omega}_d$, which we specify later in §3, i.e. $\varpi_b = \dot{\omega}_d t$. This makes forcing term in equations (8) and (9) time-dependent, but still permits analytical solution in the form $\mathbf{e}(t) = \mathbf{e}_{\text{free}}(t) + \mathbf{e}_{\text{forced}}(t)$, where

$$\begin{Bmatrix} k_{\text{free}}(t) \\ h_{\text{free}}(t) \end{Bmatrix} = e_{\text{free}} \begin{Bmatrix} \cos[(A + \dot{\omega}_d)t + \varpi_0] \\ \sin[(A + \dot{\omega}_d)t + \varpi_0] \end{Bmatrix} \quad (10)$$

and

$$\begin{Bmatrix} k_{\text{forced}}(t) \\ h_{\text{forced}}(t) \end{Bmatrix} = -e_{\text{forced}} \begin{Bmatrix} \cos \varpi_b \\ \sin \varpi_b \end{Bmatrix}, \quad (11)$$

$$e_{\text{forced}} = \frac{B}{A + \dot{\omega}_d - \dot{\omega}_b} \quad (12)$$

Thus, free eccentricity vector \mathbf{e}_{free} rotates at a rate $A + \dot{\omega}_d$ around the endpoint of vector $\mathbf{e}_{\text{forced}}$, which itself *rotates about the origin* with the rate $\dot{\omega}_b$. Setting $\dot{\omega}_d = \dot{\omega}_b = 0$ brings us back to the MN04 solution.

Planetesimals starting on circular orbits have $e_{\text{free}} = e_{\text{forced}}$ and reach the maximum eccentricity of

$$e = 2e_{\text{forced}} = \frac{2B}{A + \dot{\omega}_d - \dot{\omega}_b} \quad (13)$$

in the course of their secular evolution.

3. DISK MODEL.

Structure of circumbinary disks is different from that of protoplanetary disks around single stars. As a result of viscous evolution the latter are expected to have mass accretion rate \dot{M} independent of radius. In the case of circumbinary disk the torque due to binary stops the inward flow of matter and truncates the disk at inner radius r_{in} , interior to which Σ and \dot{M} are small. Simulations find that $r_{in} \approx 2a_b$ for binaries with mass ratio $M_s/M_p \sim 1$ (MacFadyen & Milosavljevic 2008).

Injection of angular momentum at its inner edge causes the disk to evolve into a configuration, in which the viscous angular momentum flux

$$F_J = 3\pi\nu\Sigma\Omega r^2, \quad (14)$$

rather than \dot{M} , is constant with radius (Pringle 1991; Ivanov et al. 1999; Rafikov 2012a). Detailed description of circumbinary protoplanetary disk properties will be provided elsewhere (Garmilla & Rafikov, in preparation); for the purposes of this paper we will assume that the disk is passive, i.e. heated predominantly by the combined light of the binary components. Assuming α -model for the viscosity ν one finds

$$\Sigma = \frac{F_J}{3\pi\alpha c_s^2 r^2}, \quad (15)$$

where c_s is a sound speed. If α is independent of radius, and midplane disk temperature scales as $T(r) \propto r^{-k}$, then the constant F_J disk has density profile

$$\Sigma(r) = \Sigma_{in} \left(\frac{r_{in}}{r} \right)^p, \quad p = 2 - k, \quad (16)$$

where $\Sigma_{in} \equiv \Sigma(r_{in})$. Passive disks typically have $k \approx 1/2$, in particular Chiang & Goldreich (1997) find $k = 3/7$. For this reason we will take $p = 3/2$ in this work, which is similar to the Σ slope of the Minimum Mass Solar Nebula (Hayashi 1981), and is different from $p \approx 1$ expected for a passive constant \dot{M} disk (Rafikov 2012b).

Most of the mass in a constant F_J disk is contained in its outer regions. Assuming that $p = 3/2$ profile is maintained all the way to the outer radius r_o we find that

$$\begin{aligned} \Sigma(r) &\approx \frac{M_d}{4\pi r_o^2} \left(\frac{r_o}{r} \right)^{3/2} \\ &\approx 1.3 \times 10^3 \text{ g cm}^{-2} \frac{M_d}{0.01 M_\odot} r_{o,30}^{-1/2} r_1^{-3/2}, \end{aligned} \quad (17)$$

where M_d is the disk mass, $r_{o,30} = r_o/(30\text{AU})$, $r_1 = r/(1\text{AU})$.

We show in Appendix A that disk with density profile (17) gives rise to apsidal precession of planetesimal orbits at the rate

$$\dot{\omega}_d = -\frac{\pi K_d G \Sigma(r)}{4 r n} \approx -\frac{K_d}{16} n \frac{M_d}{M_b} \left(\frac{r}{r_o} \right)^{1/2}, \quad (19)$$

(where $K_d \approx 4.4$), as well as apsidal precession of the central binary at the rate

$$\dot{\omega}_b = \frac{\pi G \Sigma_{in} \tilde{\phi}}{n_b r_{in}} \tilde{\phi} \left(\frac{a_b}{r_{in}} \right) = \frac{\tilde{\phi}}{4} n_b \frac{M_d}{M_b} \frac{a_b^3}{r_o^{1/2} r_{in}^{5/2}}, \quad (20)$$

where $\tilde{\phi} \approx 0.5$, see equation (A3).

Equation (20) assumes disk to be sharply truncated at r_{in} , while in reality Σ smoothly (but rapidly) goes to zero near r_{in} (MacFadyen & Milosavljevic 2008), which lowers the amount of mass near the binary and may reduce $\dot{\omega}_b$. To account for this we will sometimes consider wider disk cavity, e.g. $r_{in} = 3a_b$ (Pelupessy & Portegies Zwart 2012) instead of the more conventional $2a_b$.

4. PLANETESIMAL VELOCITIES.

Equation (12) shows that planetesimal eccentricity is determined by A , $\dot{\omega}_d$ and $\dot{\omega}_b$. We plot the behavior of these frequencies as a function of r in Figure 1. Using equations (5), (19) and (20) we find that

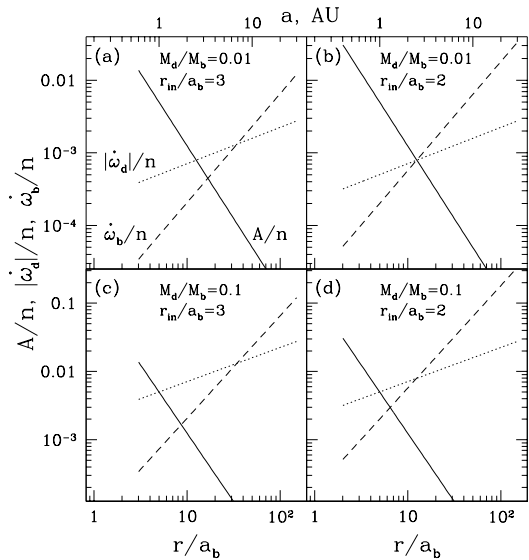


Figure 1. Characteristic precession frequencies of the problem as a function of distance from the binary (in units of a_b on the lower axis and in AU on the upper), for different values of the relative disk mass M_d/M_b and the size of the inner disk cavity r_{in}/a_b , as labeled on panels. Calculation assumes $M_b = M_\odot$, $\mu = 0.21$, $a_b = 0.2$ AU, and $e_b = 0.2$. Shown are A/n (solid), $|\dot{\omega}_d|/n$ (dotted), and $\dot{\omega}_b/n$ (dashed), marked in panel (a). Note that for small M_d/M_b and r_{in}/a_b region where $|\dot{\omega}_d|$ dominates over other frequencies disappears.

$\dot{\omega}_b/A \propto (r/a_b)^{7/2}$ and $\dot{\omega}_b/|\dot{\omega}_d| \propto r/a_b$. Both ratios increase with r so that $\dot{\omega}_b \gtrsim A$ for $r \gtrsim r_A$, where

$$\begin{aligned} \frac{r_A}{a_b} &\approx 14 \left[\frac{\mu(1-\mu)}{0.25} \frac{0.01}{M_d/M_b} \right]^{2/7} \\ &\times \left(\frac{r_{o,30}}{a_{b,0.2}} \right)^{1/7} \left(\frac{r_{in}/a_b}{2} \right)^{5/7}, \end{aligned} \quad (21)$$

with $a_{b,0.2} \equiv a_b/(0.2\text{AU})$. Also, $\dot{\omega}_b \gtrsim |\dot{\omega}_d|$ for $r \gtrsim r_d$, where (setting $K_d = 4.4$ and $\tilde{\phi} = 0.5$)

$$\frac{r_d}{a_b} \approx 12 \left(\frac{r_{in}/a_b}{2} \right)^{5/2}. \quad (22)$$

Thus, for a particular set of parameters adopted in these estimates one finds that $\dot{\omega}_b$ dominates the behavior of planetesimal eccentricity beyond $(10-20)a_b$. Depending on M_d/M_b and r_{in}/a_b there may exist intermediate region around $r \sim 10a_b$, where relative precession of the planetesimal and binary orbits is dominated by $\dot{\omega}_d$. Such region disappears for lower M_d and smaller inner cavity size r_{in} , see Figure 1b.

In Figure 2 we illustrate radial dependence of the characteristic planetesimal eccentricity $e(r)$ computed with equation (13). One feature that is obvious in these plots is the secular resonance at $\sim 1-2$ AU, where A is equal to $\dot{\omega}_b + |\dot{\omega}_d|$ and our solution presented in §2.1 breaks down. This region of enhanced excitation is quite narrow, and just outside of it $e(r)$ rapidly declines with r .

We also show in this Figure asymptotic behavior of eccentricity $e^A(r)$ found when the relative precession of planetesimal and binary orbits is dominated by the *potential of the secondary* ($A \gtrsim |\dot{\omega}_d|, \dot{\omega}_b$), see (5), (6):

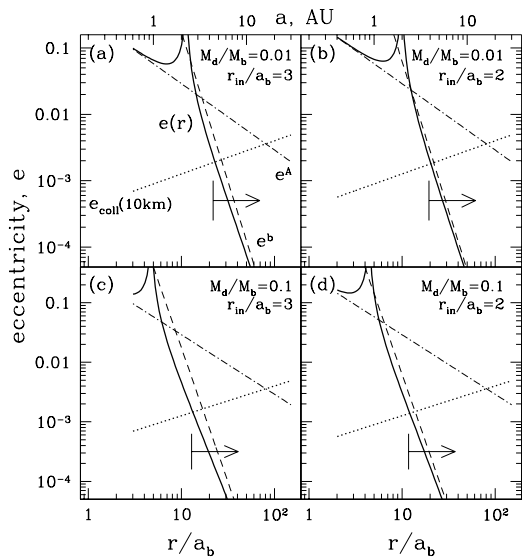


Figure 2. Maximum planetesimal eccentricity $e(r)$ (solid curve, Eq. [13]) as a function of radius, for different values of M_d/M_b and r_{in}/a_b . Dot-dashed and dashed lines illustrate asymptotic behavior of eccentricity given by e^A (Eq. [23]) and e^b (Eq. [24]). All these curves scale linearly with the binary eccentricity e_b , assumed equal to 0.2 in this calculation (also $M_b = M_\odot$, $\mu = 0.21$, $a_b = 0.2$ AU). Dotted line is the eccentricity e_{coll} (Eq. [28]) below which 10 km objects (density $\rho = 3 \text{ g cm}^{-3}$) can grow in collisions, according to the criterion (27). Planetesimal growth is unimpeded by fragmentation when $e(r) < e_{coll}(r)$ (region to the right from vertical bars with arrows).

$e \rightarrow e^A = 2B/A$, where (MN04)

$$e^A = \frac{5(1-2\mu)}{2} \frac{a_b}{r} e_b \approx 0.02(1-2\mu) \frac{25}{r/a_b} \frac{e_b}{0.2}, \quad (23)$$

and $r/a_b = 25$ is chosen so that $r = 5$ AU if $a_b = 0.2$ AU.

When relative precession is dominated by the *binary precession* ($\dot{\omega}_b \gtrsim A, |\dot{\omega}_d|$), equation (20) predicts $e \rightarrow e^b = 2B/\dot{\omega}_b$, where

$$\begin{aligned} e^b &= \frac{15\psi(\mu)}{2\tilde{\phi}} \frac{M_b}{M_d} \left(\frac{r_o}{a_b}\right)^{1/2} \left(\frac{r_{in}}{a_b}\right)^{5/2} \left(\frac{a_b}{r}\right)^{9/2} e_b \quad (24) \\ &\approx 10^{-3} \frac{\psi(\mu)}{0.1} \frac{0.01}{M_d/M_b} \left(\frac{r_{o,30}}{a_{b,0.2}}\right)^{1/2} \\ &\quad \times \left(\frac{r_{in}/a_b}{2}\right)^{5/2} \left(\frac{r/a_b}{25}\right)^{-9/2} \frac{e_b}{0.2}. \quad (25) \end{aligned}$$

Here $\psi(\mu) \equiv \mu(1-\mu)(1-2\mu)$ and for $0 < \mu < 0.5$ the maximum value of $\psi \approx 0.096$ is achieved at $\mu \approx 0.21$.

Between these two limits, at $r \sim 1$ AU, disk-driven planetesimal precession may dominate (see Figure 1), but usually marginally. For this reason we do not show asymptotic scaling for this regime.

At large separations, of order several AU, $e(r) \rightarrow e^b(r)$ and falls off very steeply with r . At these separations the simple formula (23) not accounting for the gravitational effects of the disk overestimates planetesimal eccentricity by more than an order of magnitude.

5. SHORT-PERIOD ECCENTRICITY VARIATIONS.

Planetesimal motion is affected not only by the explicitly time-independent, secular part of the disturbing function (3), but also by the short-term perturbations varying on timescales $\sim n_b^{-1}$ and n^{-1} . The former average out to zero over the planetesimal orbital motion, but the latter were suggested to affect planetesimal dynamics.

In particular, MN04 and Paardekooper et al. (2012) found that even for circular binaries ($e_b = 0$), when secular excitation is absent (see equations [6] and [13]), time-dependent contributions to the disturbing function varying on the planetesimal orbital timescale n^{-1} (i.e. averaged over the *binary* period) still result in eccentricity evolution. This result is surprising since in $e_b = 0$ case the potential of the binary averaged over the fast binary orbital timescale is time-independent and axisymmetric. Consequently, both energy and angular momentum of the planetesimal must be conserved precluding its eccentricity evolution.

The unexpected finding of MN04 and Paardekooper et al. (2012) is most likely related to their choice of a reference circular orbit and osculating orbital elements. The former was defined as the circular orbit in a Keplerian potential for the mass $M_b = M_p + M_s$. However, one can show that the true axisymmetric part of the binary (plus disk) potential to lowest order in a_b/r is

$$\begin{aligned} U_{m=0}(r) &= U_d(r) - \frac{GM_b}{r} \\ &\quad \times \left[1 + \frac{1}{4}\mu(1-\mu) \left(\frac{a_b}{r}\right)^2 \left(1 + \frac{3}{2}e_b^2\right) \right]. \quad (26) \end{aligned}$$

Circular orbits in this potential have *higher* circular speed than orbits in a Keplerian potential for mass M_b at the same distance. Thus, a particle initialized on “circular” orbit, assuming $-GM_b/r$ potential, is in fact started at the *apoapse of eccentric orbit* in the true potential (26). Not surprisingly, its orbit will remain eccentric, with eccentricity determined ultimately by the difference between the circular velocities in $U_{m=0}$ and the M_b point mass potentials. It is trivial to show that this fictitious eccentricity is $(3/4)\mu(1-\mu)(a_b/r)^2$, which is in perfect agreement with the numerical calculations of MN04 and analytical result Paardekooper et al. (2012) for $e_b = 0$. The importance of proper definition of osculating orbital elements has been previously emphasized by Marzari et al. (2008).

Careful analysis in the $e_b \neq 0$ case shows that the disturbing function contains terms varying on planetesimal orbital timescale, which formally result in eccentricity of order $\mu(1-\mu)(a_b/r)^2 e_b^2$. Even taken at face value, this eccentricity is most likely too small to affect the results in §4; whether it produces significant *relative* velocity between colliding objects is even less obvious. We leave the detailed study of the short-term eccentricity variations for the future.

6. IMPLICATIONS FOR PLANET FORMATION.

We now address the issue of fragmentation barrier for planetesimal growth. Based on work of Leinhardt & Stewart (2012) we estimate that a gravity-dominated body (e.g. a rubble pile) of radius d survives in a collision with a body of *equal size* whenever the collision

velocity v_{coll} (at large separation) satisfies a simple condition (Rafikov 2012b)

$$v_{coll} \lesssim 2v_{esc}, \quad (27)$$

where the escape speed from the surface of an object of radius d and bulk density ρ is $v_{esc} = [(8\pi/3)G\rho]^{1/2}d$. This condition is similar to the one used in MN04. It can be translated into the constraint on the maximum planetesimal eccentricity $e_{coll} \approx 2v_{esc}/v_K$ (where v_K is the Keplerian speed), at which an equal-mass collision does not result in the net loss of mass:

$$e_{coll}(r, d) \approx \left(\frac{32\pi \rho r d^2}{3 M_b} \right)^{1/2} \\ \approx 2 \times 10^{-3} \left(\frac{\rho_3}{M_{b,1}} \frac{r}{5\text{AU}} \right)^{1/2} d_{10}, \quad (28)$$

where $M_{b,1} \equiv M_b/M_\odot$, $\rho_3 \equiv \rho/(3 \text{ g cm}^{-3})$, and $d_{10} \equiv d/(10\text{km})$.

We will now assume that if (1) the characteristic planetesimal eccentricity given by equation (13) is below $e_{coll}(r, d_s)$ at some distance r and (2) planetesimals are strength-dominated below the radius d_s , then fragmentation barrier at this separation r is bypassed.

To be specific, we take $d_s = 10 \text{ km}$ in our study. This may seem somewhat large since collisionally assembled objects may be rubble piles. On the other hand, more sophisticated fragmentation criteria accounting for the size spectrum of colliding objects (i.e. incorporating more than just equal-mass collisions) typically find our survival criterion (27) too restrictive (Thébault 2011; Rafikov 2012b). This may justify relatively large value of $d_s = 10 \text{ km}$.

Figure 2 shows that with this value of d_s fragmentation barrier does not get in the way of planetesimal growth at separations $\gtrsim 2 - 4 \text{ AU}$. Inner radius of the accretion-friendly zone a_{form} depends mainly on the size of the inner cavity in the disk and to some extent on the disk mass. A rough estimate of a_{form} (typically an overestimate by up to a factor of 2) can be obtained by equating e^b and e_{coll} :

$$a_{\text{form}} \approx 22a_b \left(\frac{M_{b,1} r_{o,30}}{\rho_3} \right)^{1/10} \left(\frac{r_{in}/a_b}{2} \right)^{1/2} \\ \times \left(\frac{\psi(\mu)}{0.1} \frac{0.01}{M_d/M_b} \frac{e_b}{0.2} d_{10}^{-1} a_{b,0.2}^{-1} \right)^{1/5}. \quad (29)$$

Larger r_{in}/a_b means less disk mass near the binary and slower binary precession. Larger M_d accelerates disk-induced precession of both the planetesimal orbit and the binary. Larger value of critical planetesimal size d_s also shifts a_{form} closer to the binary.

In the absence of disk-driven precession, using e^A instead of e^b in the growth condition (27) to calculate a_{form} , we would obtain $a_{\text{form}} \approx 90a_b \approx 17 \text{ AU}$ (crossing of dotted and dot-dashed lines in Figure 2), pushing accretion-friendly zone much further from the binary, in agreement with MN04. Formation of cores massive enough to trigger core accretion ($\sim 10M_\oplus$) prior to disk dispersal is more problematic at this separation than at 2-3 AU, because of the longer dynamical timescale. Thus, by extending inward the region, where planetesimals can grow

effectively, the gravitational effect of the disk on planetesimal secular evolution facilitates circumbinary planet formation via the reduction of the planetary accretion timescale.

In Table 1 we show a_{form} computed using parameters of actual *Kepler* circumbinary planetary systems. Minimum and maximum values shown correspond to $M_d/M_b = 0.1$, $r_{in}/a_b = 2$ and $M_d/M_b = 0.01$, $r_{in}/a_b = 3$, correspondingly. In Kepler-47 system² secular excitation is additionally suppressed because $e_b = 0.02 \ll 1$ (Orosz et al. 2012a). In Kepler-34 and Kepler-35 it is reduced because μ is very close to 0.5: $\mu = 0.493$ and 0.477, correspondingly (Welsh et al. 2012). Compared to the nominal $\mu = 0.2$ case, we find e^A in these systems to be suppressed by ≈ 40 and ≈ 13 , respectively, while e^d and e^b are lowered by ≈ 27 and 9, correspondingly. This shifts accretion-friendly zone closer to the binary.

Nevertheless, even accounting for the gravitational effect of the disk, in-situ formation still does not seem viable for the *Kepler* circumbinary planets, which have $a_{\text{form}} > a_{pl}$ (Table 1). Thus, some form of inward migration is still needed to deliver these planets to their current locations.

We also note that gas drag is not important for resolving the fragmentation barrier issue in Kepler circumbinary systems: fast relative precession of planetesimal and binary orbits (mainly due to $\dot{\omega}_b \gg A$) makes planetesimal apsidal alignment inefficient, contrary to standard expectation without disk gravity (Scholl et al. 2007). Calculations similar to the one in Rafikov (2012b) demonstrate that gas drag regulates eccentricity behavior at 2-3 AU only for bodies smaller than 1 km, which is below our adopted threshold size d_s .

However, gas drag may have detrimental effect on circumbinary planet formation if the turbulence (Meschiari 2012b) or the density waves driven by the binary in the disk (Marzari et al. 2008) can strongly excite planetesimal eccentricities at large r/a_b . Drag-induced inspiral of solids is another possible obstacle for planet formation. We leave detailed exploration of these issues to future study.

This work was supported by NSF via grant AST-0908269.

REFERENCES

- Chiang, E. I. & Goldreich, P. 1997, *ApJ*, 490, 368
 Cieza, L. A., et al. 2009, *ApJ*, 696, L84
 Doyle, L. R., et al. 2011, *Science*, 333, 1602
 Hayashi, C. 1981, *Prog. Theor. Phys. Suppl.*, 70, 35
 Holman, M. J. & Wiegert, P. A. 1999, *AJ*, 117, 621
 Ivanov, P. B., Papaloizou, J. C. B., & Polnarev, A. G. 1999, *MNRAS*, 307, 79
 Leinhardt, Z. M. & Stewart, S. T. 2012, *ApJ*, 745, id. 79
 Kraus, A. L., Ireland, M. J., Hillenbrand, L. A., & Martinache, F. 2012, *ApJ*, 745, id. 19
 MacFadyen, A. I. & Milosavljevic, M. 2008, *ApJ*, 672, 83
 Marzari, F., Thébault, P., & Scholl, H. 2008, *ApJ*, 681, 1599
 Meschiari, S. 2012a, *ApJ*, 752, 71
 Meschiari, S. 2012b, arXiv:1210.7757
 Moriwaki, K. & Nakagawa, Y. 2004, *ApJ*, 609, 1065 (MN04)
 Murray, C. D. & Dermott, S. F. 1999, *Solar System Dynamics*, Cambridge University Press; Cambridge
 Orosz, J. A., et al. 2012a, *Science*, 337, 1511

² Equation (29) works poorly for this system because of large $\dot{\omega}_d$.

Orosz, J. A., et al. 2012b, ApJ, 758, id. 87
 Paardekooper, S.-J., Leinhardt, Z. M., Thébault, P., & Baruteau, C. 2012, ApJ, L16
 Pelupessy, F. I. & Portegies Zwart, S. 2012, arXiv:1210.4678
 Pringle, J. E. 1991, MNRAS, 248, 754
 Rafikov, R. R. 2012a, arXiv:1205.5017
 Rafikov, R. R. 2012b, arXiv:1212.1465

Scholl, H., Marzari, F., & Thébault, P. 2007, MNRAS, 380, 1119
 Schwamb, M. E., et al. 2012, arXiv:1210.3612
 Thébault, P. 2011, Cel. Mech. Dyn. Astr., 111, 29
 Ward, W. R. 1981, Icarus, 47, 234
 Welsh, W. F., et al. 2012, Nature, 481, 475

APPENDIX

DISK-INDUCED PRECESSION RATES.

Potential U_d of an axisymmetric disk with a power-law surface density profile in the form (16), truncated at the inner radius r_{in} (i.e. $\Sigma(r) = 0$ for $r < r_{in}$) is given by the following expression far from the inner edge of the disk, $r \gg r_{in}$ (Ward 1981):

$$U_d(r) \approx -2\pi K_d G \Sigma_{in} \left(\frac{r_{in}}{r}\right)^p r, \quad K_d = \sum_{l=0}^{\infty} \frac{A_l(4l+1)}{(2l+p-1)(2l-p+2)} \approx 4.4, \quad (\text{A1})$$

where $A_l = [(2l)!/(2^{2l}(l!)^2)]^2$, and the numerical value of K_d is for $p = 3/2$. Substituting this expression into equation (4), assuming $p = 3/2$ and using equation (17), we arrive at the result (19).

To calculate apsidal precession of the binary we use the expression for U_d inside the inner edge ($r < r_{in}$) of a sharply truncated disk (Ward 1981):

$$U_d(r) = -2\pi G \Sigma_{in} r_{in} \phi \left(\frac{r}{r_{in}}\right), \quad \phi(z) = \sum_{l=0}^{\infty} \frac{A_l z^{2l}}{2l+p-1}. \quad (\text{A2})$$

Taking into account that both stars move in this potential one can show using equation (4) that binary precesses at the rate (20) with

$$\tilde{\phi}(z) = \sum_{l=1}^{\infty} A_l \frac{2l(2l+1)}{2l+p-1} [\mu^{2l} + (1-\mu)^{2l}] z^{2(l-1)}, \quad (\text{A3})$$

where equation (17) was used. We numerically found that $\tilde{\phi} \approx 0.3 - 0.8$ for $a_b/r_{in} = 0.3 - 0.5$ and $\mu = 0 - 0.5$. For simplicity, in this study we simply set $\tilde{\phi} \approx 0.5$.